

Electronic States and Local Density of States in Graphene with a Corner Edge Structure

Yuji SHIMOMURA, Yositake TAKANE, and Katsunori WAKABAYASHI^{1,2}

*Department of Quantum Matter, Graduate School of Advanced Sciences of Matter,
Hiroshima University, Higashihiroshima, Hiroshima 739-8530, Japan*

¹*International Center for Materials Nanoarchitectonics (MANA), National Institute for Materials
Science (NIMS), Namiki, Tsukuba 305-0044, Japan*

²*PRESTO, Japan Science and Technology Agency, Kawaguchi 332-0012, Japan*

(Received)

We study electronic states of semi-infinite graphene with a corner edge, focusing on the stability of edge localized states at zero energy. The 60°, 90°, 120° and 150° corner edges are examined. The 60° and 120° corner edges consist of two zigzag edges, while 90° and 150° corner edges consist of one zigzag edge and one armchair edge. We numerically obtain the local density of states (LDOS) on the basis of a nearest-neighbor tight-binding model by using Haydock's recursion method. We show that edge localized states appear along a zigzag edge of each corner edge structure except for the 120° case. To provide insight into this behavior, we analyze electronic states at zero energy within the framework of an effective mass equation. The result of this analysis is consistent with the behavior of the LDOS.

KEYWORDS: graphene corner edge, localized state, zigzag edge, armchair edge, tunneling spectroscopy

1. Introduction

The realization of a monolayer graphene sheet^{1,2)} has triggered extensive studies on its unusual electronic properties arising from the two-dimensional honeycomb structure of carbon atoms.³⁾ Since the unit cell of the honeycomb lattice contains two nonequivalent sites which form two sublattices A and B, the low-energy electronic states of graphene near the Fermi energy are described by a 2×2 matrix form which is equivalent to the massless Dirac equation.⁴⁾ Thus, electrons in graphene are called massless Dirac fermions. The band structure of massless Dirac fermions has a unique character, since they have linear energy dispersion in the vicinity of two nonequivalent symmetric points, called K^+ and K^- points, in the Brillouin zone, where the conduction and valence bands conically touch.⁵⁾ This structure is called Dirac cone. We hereafter set the electron energy at the band touching point as $\varepsilon = 0$. The unique energy band structure provide a number of intriguing physical properties such as the half-integer quantum Hall effect,^{2,6)} the absence of backward scattering associated with the Berry's phase by π ⁷⁾ and Klein tunneling.⁸⁾

The presence of edges makes an strong impact on the Dirac fermions in graphene near

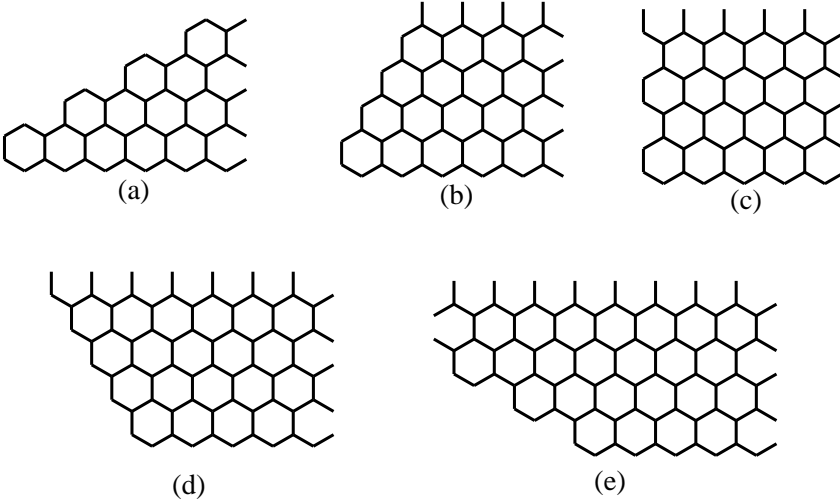


Fig. 1. Typical corner edge structures with corner angles of (a) 30° , (b) 60° , (c) 90° , (d) 120° and (e) 150° .

the Fermi energy. As stressed by Fujita *et al.*, the electronic states near the graphene edge strongly depends on its edge orientation.⁹⁾ Typical straight edges of graphene are classified into two structures: one is zigzag (zz) edge and the other is armchair (ac) edge. Fujita *et al.* analyzed electronic states in graphene with an infinitely long straight edge on the basis of a nearest-neighbor tight-binding model, and showed that highly degenerate edge localized states appear at $\varepsilon = 0$ along a zz edge.⁹⁾ These states at $\varepsilon = 0$ result in a sharp zero-energy peak structure in the local density of states (LDOS) near a straight zz edge of graphene. The edge localized states have a characteristic feature that their probability amplitude is finite only on one sublattice including edge sites and completely vanishes on the other sublattice. No such localized states appear along an ac edge. The presence of edge localized states along a zz edge has been confirmed by using scanning tunneling microscopy and scanning tunneling spectroscopy.^{10, 11)}

Theoretically, the presence or absence of zero-energy localized states has been well understood for infinitely long straight edges. However, actual edges of graphene samples are never straight nor infinitely long, and are much more complex than ideal ones. An actual edge line consists of several zz and/or ac segments, and a corner edge inevitably appears at the boundary of two adjacent segments. Typical corner edge structures are shown in Fig. 1. Hereafter each corner edge is referred to according to its corner angle. The 30° , 90° , and 150° corner edges consist of one zz edge and one ac edge, while the 60° and 120° corner edges consist of two zz edges. There arises a natural question: Do edge localized states exist at $\varepsilon = 0$ along a bent edge of these corner edge structures? In this paper we study electronic states in the corner edge structures to answer this question. We adopt a nearest-neighbor tight-binding model and numerically obtain the LDOS by using Haydock's recursion method. We find that edge

localized states appear along a zz edge of each corner edge structure with an exception of the 120° corner edge. In the 120° case, edge localized states locally disappear near the corner but emerge with increasing the distance from the corner. To provide insight into these unexpected behaviors, we analyze electronic states at $\varepsilon = 0$ within the framework of an effective mass equation. The result of this analysis is consistent with the behavior of the LDOS.

2. Formulations for Numerical Analysis

2.1 Model of graphene corner edges

We describe π electrons in graphene with a corner edge structure by using a tight-binding model on a honeycomb lattice. The Hamiltonian of this model is represented as

$$H = -t \sum_{\langle i,j \rangle} |i\rangle\langle j| + \sum_i w_i |i\rangle\langle i|, \quad (1)$$

where t is the nearest neighbor hopping integral and w_i is a site-dependent potential. If $w_i = 0$ for any i , this model corresponds to a bulk graphene sheet. The site-dependent potential w_i is introduced for a technical reason. For practical application of our numerical approach, it is convenient to treat a lattice system being infinite in both the longitudinal and transverse directions. However, such a system contains lattice sites which are irrelevant for a corner edge structure. To model a corner edge on this infinite system, we put a large on-site potential on each irrelevant site to prevent electrons arriving on it. Therefore, we set $w_i = w$ with a sufficiently large w if the i th site is irrelevant for a corner edge structure while $w_i = 0$ otherwise.

We consider four corner edges having corner angles differ from each other. The angles are 60°, 90°, 120° and 150°. We particularly focus on corner edges including one or two zz edges.

2.2 Haydock's recursion method

The LDOS can be calculated with Haydock's recursion method^{12–15)} which is applicable to systems having no translational symmetry such as graphene with a corner edge. By applying this method, we can obtain the LDOS at an arbitrary site.

We outline the method to obtain the LDOS at an i th site. To start with, we transform our model to a one-dimensional chain model. We first introduce the coefficient a_0 given by

$$a_0 = \langle l_0 | H | l_0 \rangle \quad (2)$$

with $|l_0\rangle \equiv |i\rangle$, and define $|l_1\rangle$ and b_1 in terms of

$$b_1 |l_1\rangle = (H - a_0) |l_0\rangle \quad (3)$$

with $\langle l_1 | l_1 \rangle \equiv 1$. The coefficient b_1 is obtained as

$$b_1 = \sqrt{\langle l_0 | (H - a_0)(H - a_0) | l_0 \rangle}. \quad (4)$$

We next introduce a_1 given by

$$a_1 = \langle l_1 | H | l_1 \rangle, \quad (5)$$

and define $|l_2\rangle$ and b_2 in terms of

$$b_2 |l_2\rangle = (H - a_1) |l_1\rangle - b_1 |l_0\rangle \quad (6)$$

with $\langle l_2 | l_2 \rangle \equiv 1$. The coefficient b_2 is obtained as

$$b_2 = \sqrt{\{ \langle l_1 | (H - a_1) - \langle l_0 | b_1 \} \{ (H - a_1) |l_1\rangle - b_1 |l_0\rangle \}}. \quad (7)$$

Repeating this n times, we obtain

$$b_{n+1} |l_{n+1}\rangle = (H - a_n) |l_n\rangle - b_n |l_{n-1}\rangle, \quad (8)$$

with

$$a_n = \langle l_n | H | l_n \rangle, \quad (9)$$

$$b_{n+1} = \sqrt{\{ \langle l_n | (H - a_n) - \langle l_{n-1} | b_n \} \{ (H - a_n) |l_n\rangle - b_n |l_{n-1}\rangle \}}. \quad (10)$$

This manipulation with the recurrence equation, eq. (8), is equivalent to a transformation of the original electron system to a one-dimensional chain model. $\{|l_0\rangle, |l_1\rangle, |l_2\rangle, \dots\}$ stands for the orthonormal basis set of the chain model. Here, $|l_n\rangle$ involves neighboring sites of $|i\rangle$ up to the n th nearest neighbors. On this basis, H can be rewritten with real coefficients $\{a_0, a_1, \dots\}$ and $\{b_1, b_2, \dots\}$ as a tridiagonal matrix

$$H = \begin{pmatrix} a_0 & b_1 & & & \\ b_1 & a_1 & b_2 & & \\ & b_2 & a_2 & b_3 & \\ & & b_3 & a_3 & \\ & & & & \ddots \end{pmatrix}. \quad (11)$$

With the coefficients $\{a_0, a_1, \dots\}$ and $\{b_1, b_2, \dots\}$, the Green's function $G_i(E)$ for the i th site can be represented as a continued fraction,

$$G_i(E) = \cfrac{1}{E - a_0 - \cfrac{b_1^2}{E - a_1 - \cfrac{b_2^2}{\dots}}}. \quad (12)$$

Practically, we need to terminate this continued fraction at a sufficiently large n . If it is terminated at $n = N$, we obtain the approximate expression of $G_i(E)$ as

$$G_i(E) = \cfrac{1}{E - a_0 - \cfrac{b_1^2}{E - a_1 - \cfrac{b_2^2}{\dots - \cfrac{b_N^2}{E - a_N - t(E)}}}}, \quad (13)$$

where

$$t(E) = \frac{E - a_N}{2b_N^2} \left[1 - \left\{ 1 - \frac{4b_N^2}{(E - a_N)^2} \right\}^{\frac{1}{2}} \right]. \quad (14)$$

$G_i(E)$ gives the LDOS at the i th site in terms of the relation

$$N_i(E) = \frac{1}{\pi} \text{Im}G_i(E - i\delta), \quad (15)$$

where δ is a positive infinitesimal. In actual numerical calculations, we treat δ as a sufficiently small but finite constant.

3. The LDOS

3.1 The LDOS in the presence of a single edge

To confirm the validity of our approach using the recursion method, we calculate the LDOS in the presence of an ideal single zz or ac edge. We set $N = 1000$, $w/t = 300$ and $\delta/t = 0.01$ throughout this paper. We first consider the case with a single zz edge. The site indices in the unit cell are given in Fig. 2(a). We display the LDOS at the sites 1, 2, 3, and 4 in Fig. 2(b)-(e). A peak at $\varepsilon = 0$ exists at the site 1 on the zz edge. The LDOS also possesses a zero-energy peak at sites on the sublattice which includes the site 1. We see that the peak decays with increasing the distance from the edge. At the sites belonging to the other sublattice, such as the site 2, a peak does not appear at $\varepsilon = 0$. These results are consistent with the presence of edge states at $\varepsilon = 0$. The decay of the zero-energy peak reflects the fact that an edge state has a finite penetration depth.

We next consider the case with a single ac edge. Figure 3 shows the LDOS in the presence of a single ac edge. We do not observe a peak of the LDOS at $\varepsilon = 0$. This is consistent with the absence of edge state in the single ac edge case.

3.2 The LDOS in the presence of a corner edge

(i) 60° corner edge.- Figure 4 shows the LDOS at several sites in the presence of the 60° corner edge consisting of two zz edges. From this figure, we can see the appearance of edge states at $\varepsilon = 0$. As shown in Fig. 4(b) and (e), a zero-energy peak exists at the sites 7 and 10 belonging to a same sublattice. Let us compare the LDOS at the site 10 (Fig. 4(e)) with that at the site 4 in the single zz edge case (Fig. 2(e)). Note that the distance from the zz edge to the site of our interest is equivalent in both the cases. We observe that the peak of the LDOS at the site 10 is higher than that at the site 4 in the single zz edge case. We consider that this enhancement of the zero-energy peak at the site 10 is caused by a superposition of edge states at one zz edge and those at the other edge, i.e. constructive interference between two edge states.

(ii) 90° corner edge.- Figure 5 shows the LDOS at several sites in the presence of the 90° corner edge. From this figure, we see that edge states appear at $\varepsilon = 0$. As shown in Fig. 5(b), (d), and (e), a zero-energy peak exists at the sites 11, 13 and 14 belonging to a same sublattice. Thus, the LDOS near the corner possesses both the character of the LDOS in the single zz edge case and that in the single ac edge case. Let us focus on the LDOS at the site

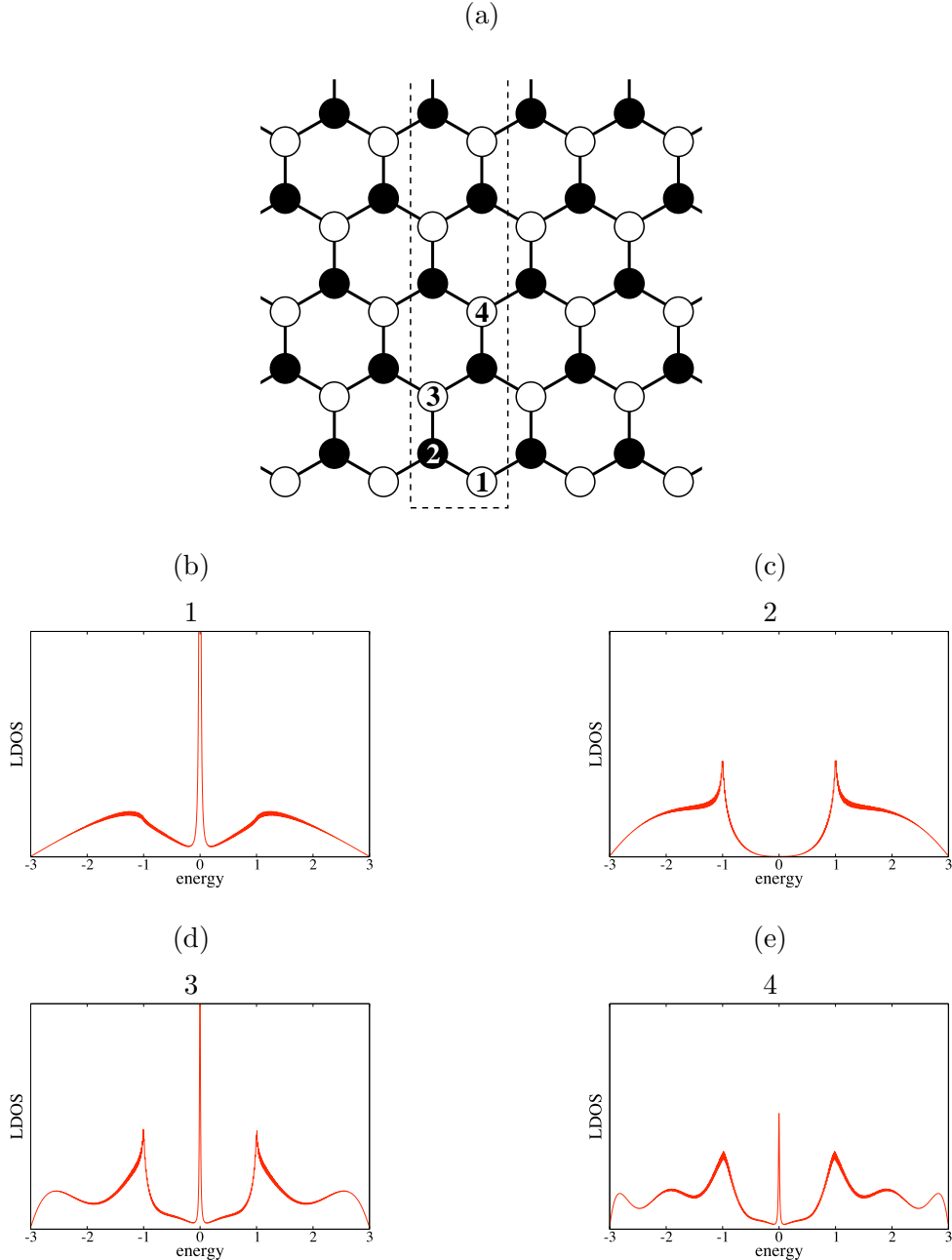


Fig. 2. (a) The structure of a single zz edge. A broken line represents a unit cell. (b), (c), (d) and (e) display the LDOS at the site 1, site 2, site 3, and site 4, respectively. The number indicated above each graph represents the site number defined in (a).

13 for example. The site 13 corresponds to the site 3 in the zz edge case (Fig. 2(d)) and the site 5 in the single ac edge case (Fig. 3(b)). Roughly speaking, we can regard that the LDOS at the site 13 (Fig. 5(d)) is a mixture of the LDOS at the site 3 (Fig. 2(d)) and the site 5 (Fig. 3(b)). The nature similar to this is also observed at other sites. There is no enhancement of the zero-energy peak of LDOS in contrast to the 60° case.

(iii) 120° corner edge.- Figure 6 shows the LDOS at several sites in the presence of the 120°

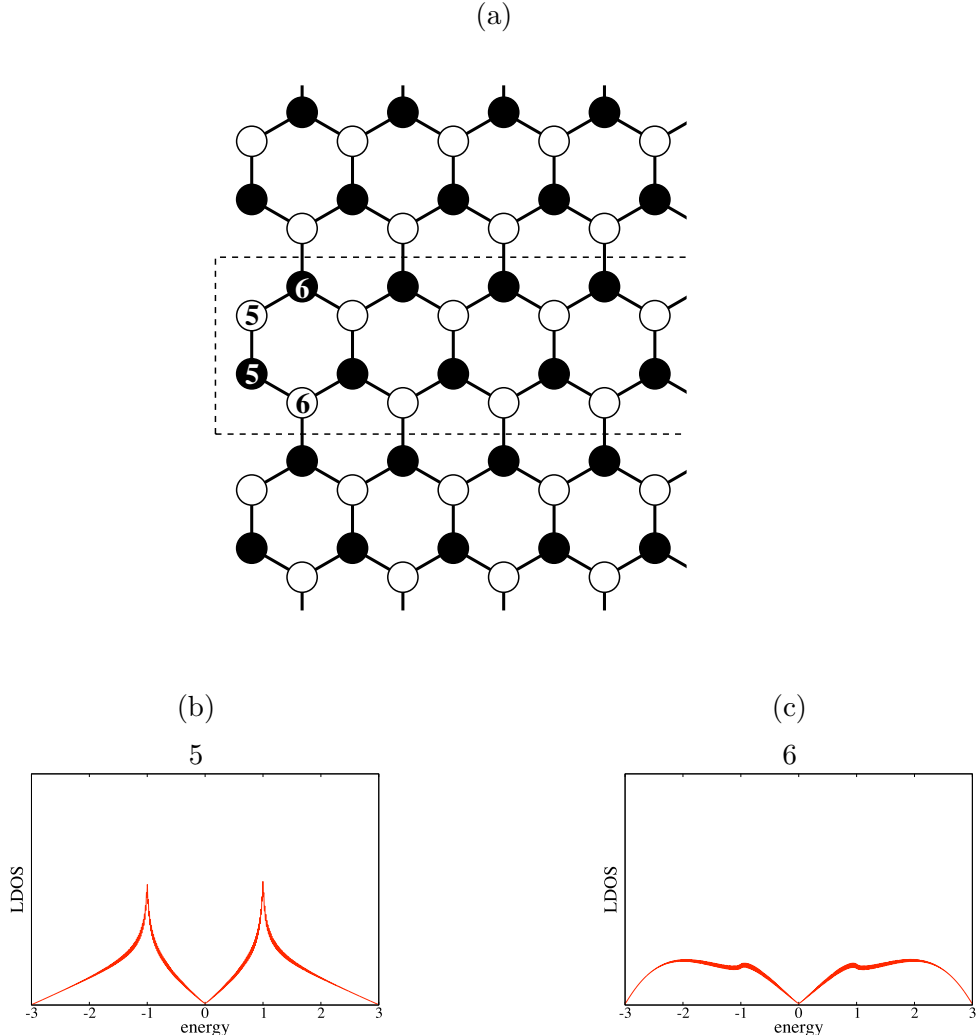


Fig. 3. (a) The structure of a single ac edge. A broken line represents a unit cell. (b) and (c) display the LDOS at the site 5 and site 6, respectively. The number indicated above each graph represents the site number defined in (a).

corner consisting of two zz edges. In this case, peculiar features arise. The LDOS at the site 15 (Fig. 6(b)) is quite different from that of the site 1 in the single zz edge case (Fig. 2(b)). As seen from Fig. 6(b), (c), and (g), there is no zero-energy peak at the sites near the corner and hence edge states locally disappear. However, edge states appear at the sites away from the corner. Indeed we observe a broad peak at the site 17 (Fig. 6(d)), and the LDOS at the site 18 (Fig. 6(e)) shows a sharp peak.

(iv) 150° corner edge.- Figure 7 shows the LDOS at several sites in the presence of the 150° corner edge. As shown in Fig. 7(b), (d), and (e), a zero-energy peak exists at the sites 21, 23 and 24 belonging to a same sublattice. This indicates the existence of edge states. As in the 90° case, the LDOS near the corner possesses both the character of the LDOS in the single zz edge case and that in the single ac edge case. For example, we can regard that the LDOS

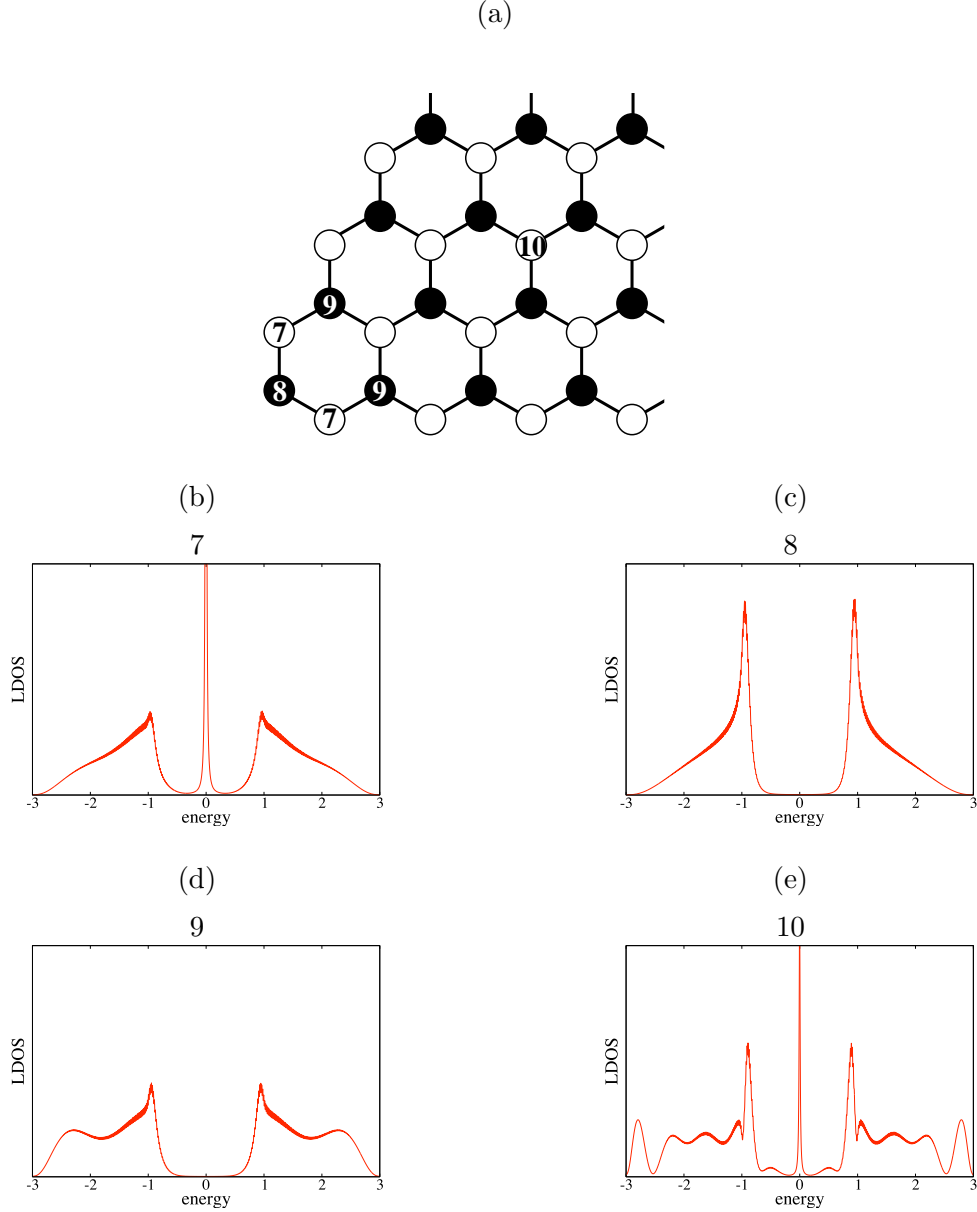


Fig. 4. (a) The structure of the 60° corner edge. (b), (c), (d) and (e) display the LDOS at the site 7, site 8, site 9, and site 10, respectively. The number indicated above each graph represents the site number defined in (a).

at the site 24 (Fig. 7(e)) is a mixture of the LDOS at the site 4 on the single zz edge (Fig. 2(e)) and that at the site 6 on the single ac edge (Fig. 3(c)). The peculiarity of the 150° case is that the zero-energy peak of the site 21 is quite smaller than that at the site 1 on the single zz edge (Fig. 2(b)).

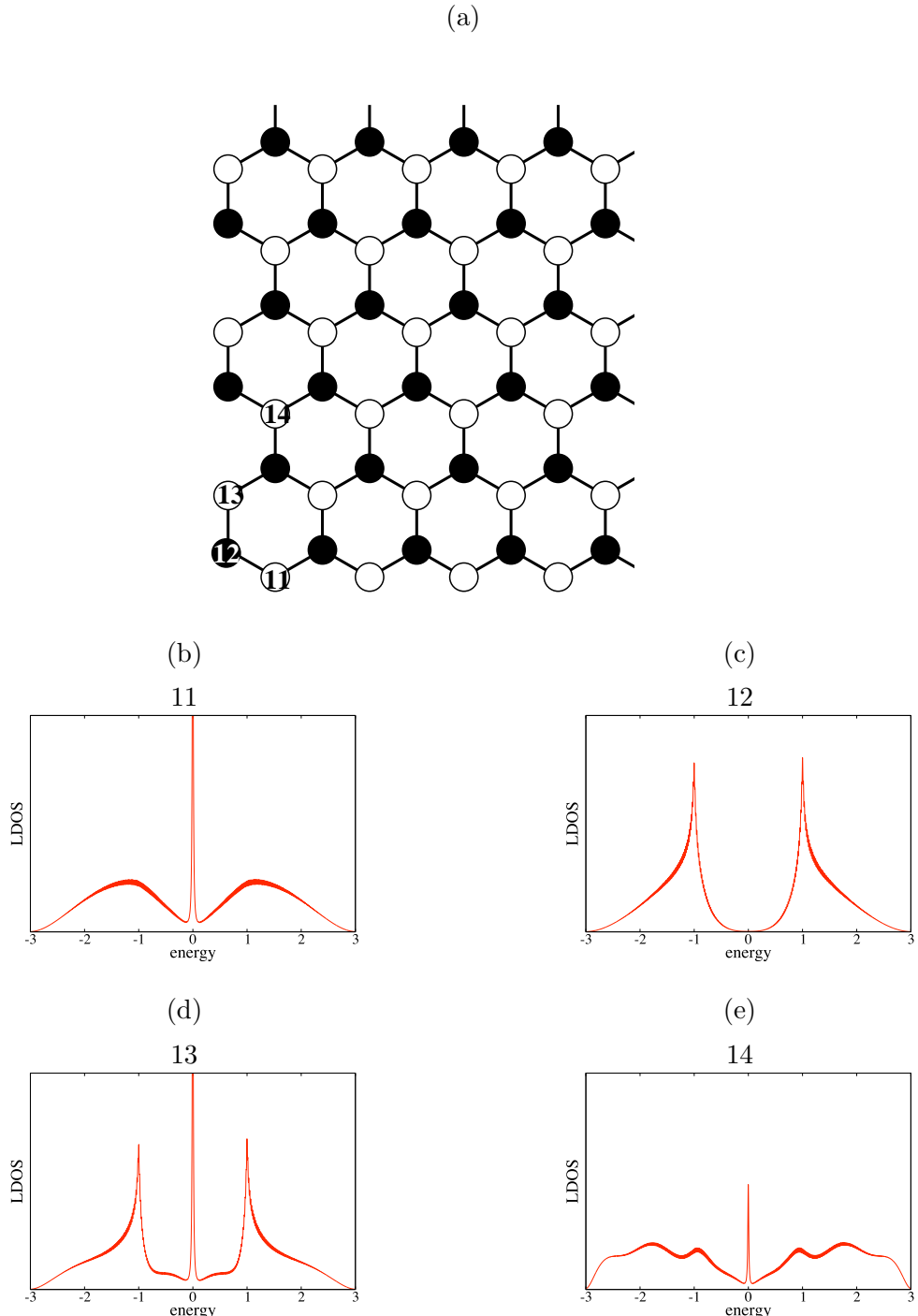


Fig. 5. (a) The structure of the 90° corner edge. (b), (c), (d) and (e) display the LDOS at the site 11, site 12, site 13, and site 14, respectively. The number indicated above each graph represents the site number defined in (a).

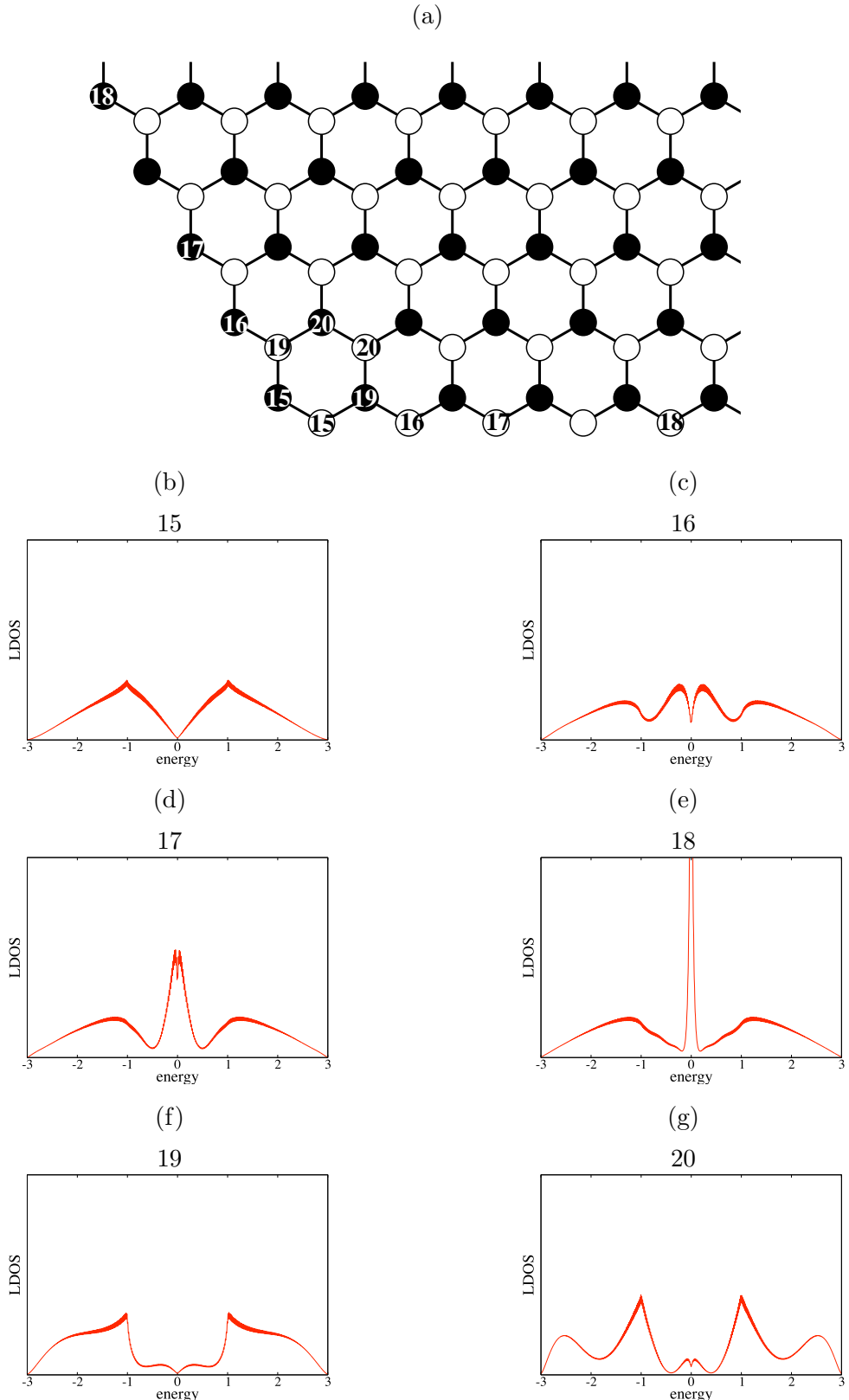


Fig. 6. (a) The structure of the 120° corner edge. (b), (c), (d), (e), (f), and (g) display the LDOS at the site 15, site 16, site 17, site 18, site 19, and site 20, respectively. The number indicated above each graph represents the site number defined in (a).

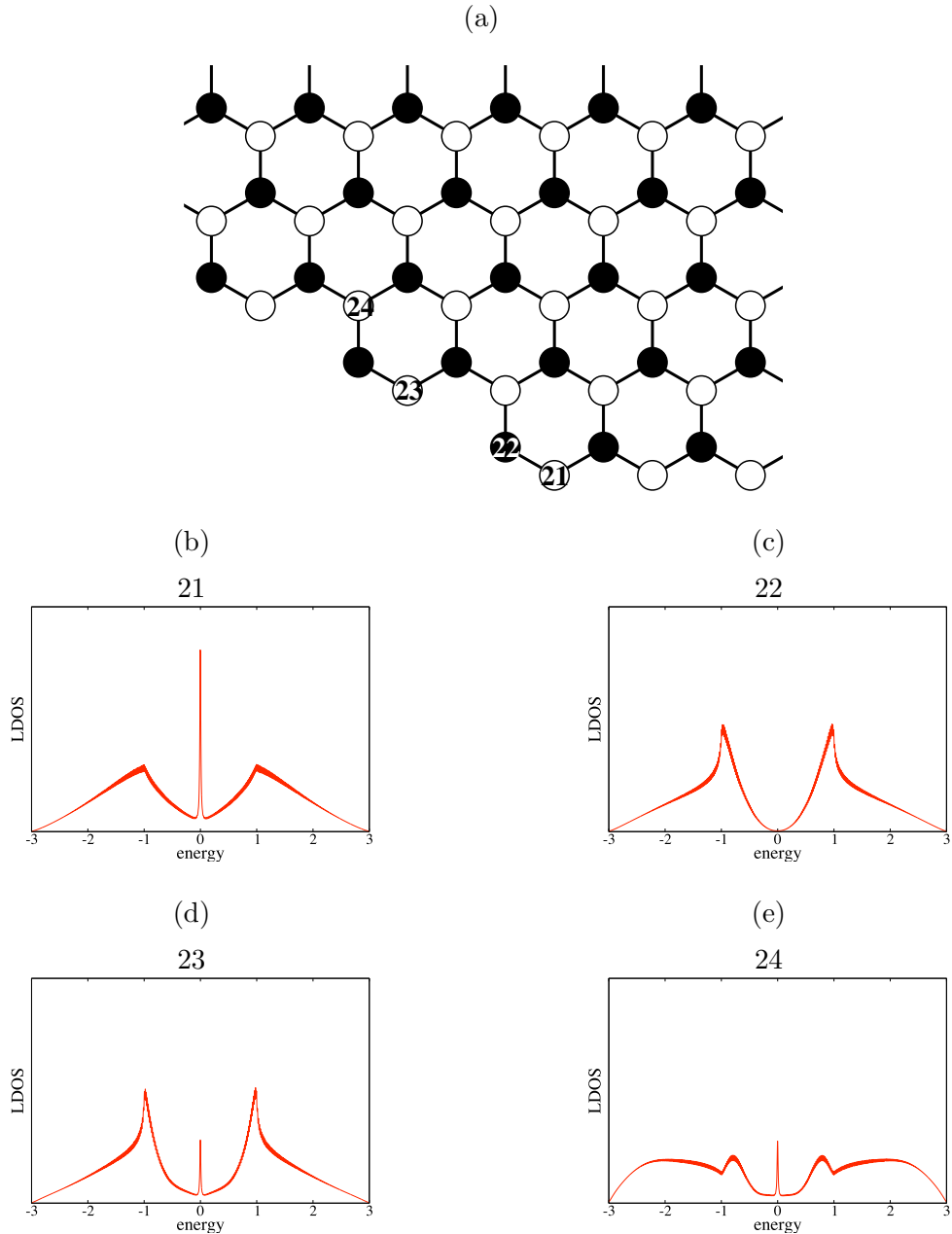


Fig. 7. (a) The strcture of the 150° corner edge. (b), (c), (d), and (e) display the LDOS at the site 21, site 22, site 23, and site 24, respectively. The number indicated above each graph represents the site number defined in (a).

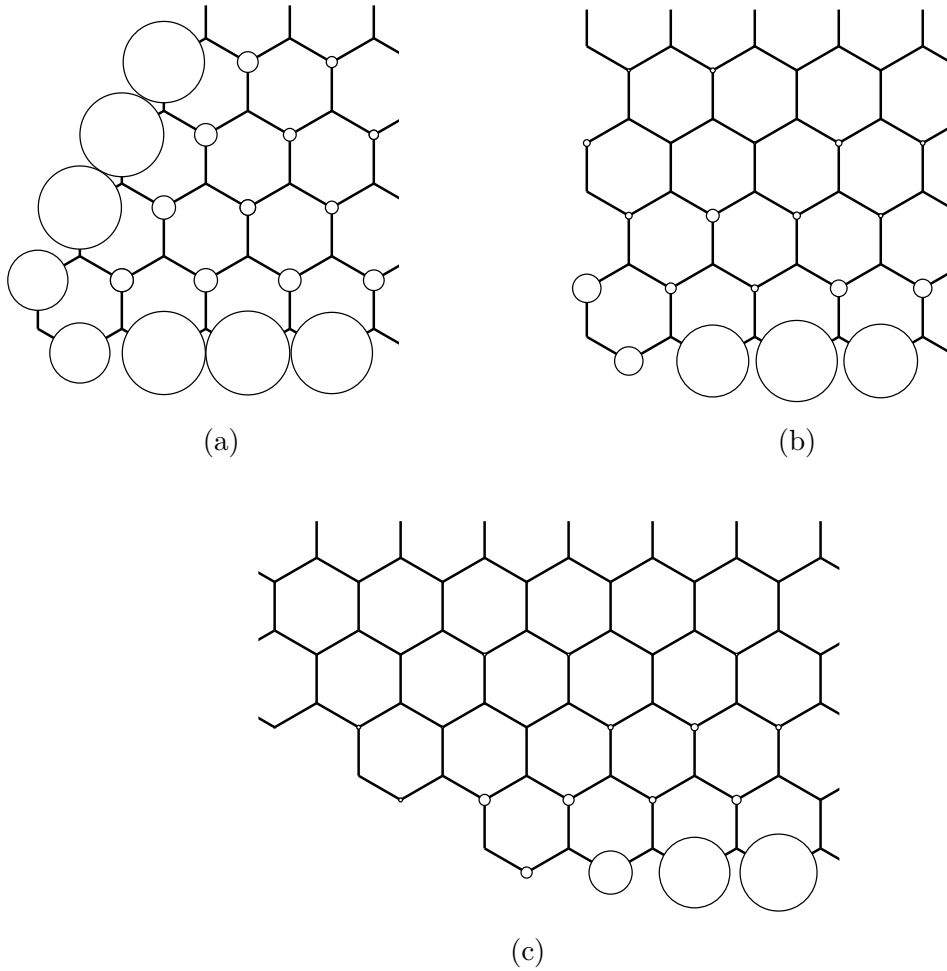


Fig. 8. The LDOS in the presence of the (a) 60° , (b) 90° and (c) 150° corner edges at $\varepsilon = 0$. The radius of open circles indicates the magnitude of the LDOS.

Figure 8 represents the spatial dependence of the LDOS at $\varepsilon = 0$ in the presence of the (a) 60° , (b) 90° , and (c) 150° corner edges. A radius of each open circle indicates the magnitude of the LDOS. In these figures, the LDOS has a finite value only on the sublattice involving zz edge sites but vanishes on the other sublattice. We observe that the LDOS localizes near zz edges, indicating the presence of edge localized states. However, special emphasis is placed on the case of the 60° corner edge, where the magnitude of the LDOS at inner sites is larger than that in the other two cases. This reflects the fact that edge localized states are present at both the two zz edges. The overlap of these edge localized states enhances the magnitude of the LDOS, i.e. constructive interference. The other corner edge structures with the angle 90° or 150° consist of one zz edge and one ac edge. Note the LDOS in the single ac edge system vanishes at $\varepsilon = 0$ on any sites. In these corner edge structures, the LDOS becomes finite even at $\varepsilon = 0$ due to the presence of a zz edge. Even at sites on the ac edge, the LDOS can have a

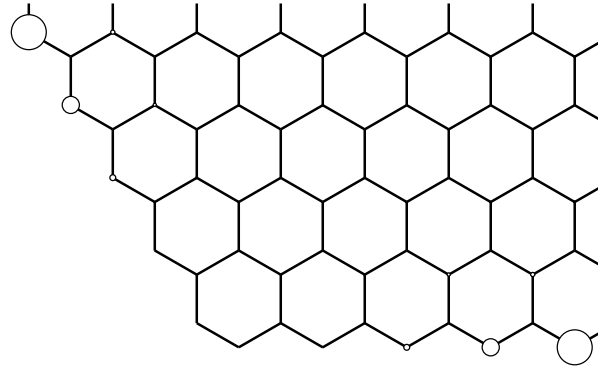


Fig. 9. The LDOS in the presence of the 120° corner edge at $\varepsilon = 0$. The radius of open circles indicates the magnitude of the LDOS.

finite value.

Figure 9 represents the spatial dependence of the LDOS at $\varepsilon = 0$ in the presence of the 120° corner edge. In this figure, we observe that the LDOS vanishes at the sites near the corner, indicating local disappearance of edge states, i.e. destructive interference. In spite of the fact that the 120° corner edge consists of two zz edges, the edge states are not fully stabilized in contrast to the case of the 60° corner edge. Note that in the 120° case, edge sites on one zz edge and those on the other zz edge belong to different sublattices, while all edge sites in the 60° case belong to a same sublattice. As we discuss in the next section, this is the reason for the qualitative difference between the two cases.

4. Analytical Treatment

Our study on the LDOS reveals that edge localized states are stabilized in corner edge structures except for the 120° case. To provide insight into this behavior, we analyze edge localized states in corner edge structures by using an effective mass description, which is applicable to low-energy states in the vicinity of the K^\pm point. The K^+ and K^- points are characterized by $\mathbf{K}^+ = (-4\pi/3a, 0)$ and $\mathbf{K}^- = (4\pi/3a, 0)$, respectively. Here, a is lattice constant. As shown in Fig. 10 (a), the unit cell of graphene has two non-equivalent carbon atoms A and B which form A sublattice and B sublattice, respectively. We represent the wave function $\psi_A(\mathbf{r})$ for A sublattice and the wave function $\psi_B(\mathbf{r})$ for B sublattice as

$$\psi_A(\mathbf{r}) = e^{i\mathbf{K}^+\cdot\mathbf{r}} F_A^+(\mathbf{r}) + e^{i\mathbf{K}^-\cdot\mathbf{r}} F_A^-(\mathbf{r}), \quad (16)$$

$$\psi_B(\mathbf{r}) = e^{i\mathbf{K}^+\cdot\mathbf{r}} F_B^-(\mathbf{r}) - e^{i\mathbf{K}^-\cdot\mathbf{r}} F_B^+(\mathbf{r}), \quad (17)$$

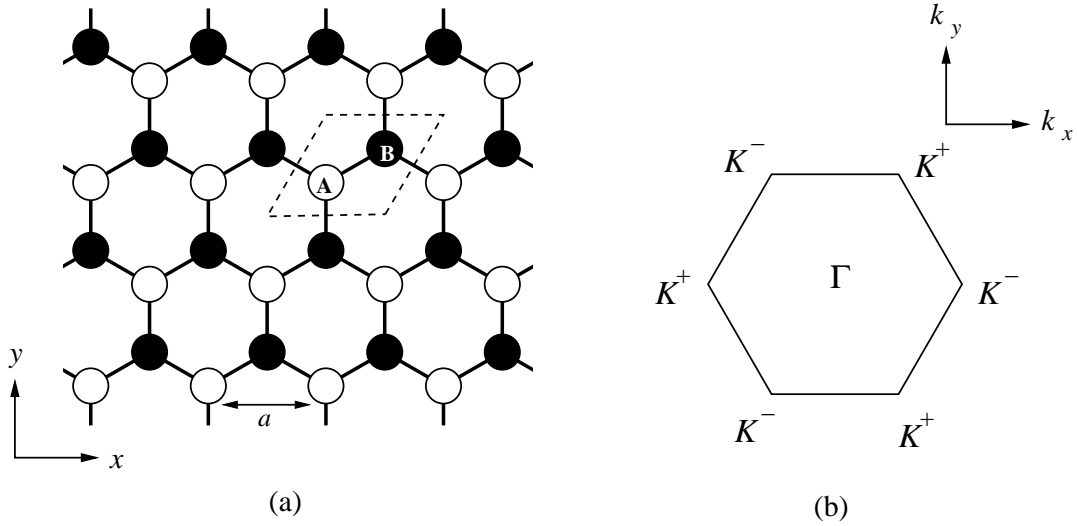


Fig. 10. (a) Honeycomb structure of graphene. The region enclosed in a broken line is a unit cell. A and B are non-equivalent sites which form sublattices. (b) The first Brillouin zone of graphene, where K^+ , K^- and Γ are symmetric points. The K^+ point is located at $(-4\pi/3a, 0)$ and $(2\pi/3a, \pm 2\pi/\sqrt{3}a)$ while the K^- point is located at $(4\pi/3a, 0)$ and $(-2\pi/3a, \pm 2\pi/\sqrt{3}a)$.

where F^\pm are envelope functions near the K^\pm point. The envelope functions at energy ε satisfy

$$\gamma \begin{pmatrix} 0 & \hat{k}_x - i\hat{k}_y & 0 & 0 \\ \hat{k}_x + i\hat{k}_y & 0 & 0 & 0 \\ 0 & 0 & 0 & \hat{k}_x + i\hat{k}_y \\ 0 & 0 & \hat{k}_x - i\hat{k}_y & 0 \end{pmatrix} \begin{pmatrix} F_A^+(\mathbf{r}) \\ F_B^+(\mathbf{r}) \\ F_A^-(\mathbf{r}) \\ F_B^-(\mathbf{r}) \end{pmatrix} = \varepsilon \begin{pmatrix} F_A^+(\mathbf{r}) \\ F_B^+(\mathbf{r}) \\ F_A^-(\mathbf{r}) \\ F_B^-(\mathbf{r}) \end{pmatrix}, \quad (18)$$

where γ is a band parameter, $\hat{k}_x = -i\partial/\partial x$, and $\hat{k}_y = -i\partial/\partial y$. This is called $\mathbf{k}\cdot\mathbf{p}$ equation,^{4,16)} which is an effective mass equation for graphene systems.

For later convenience, we present the envelope functions for edge states at $\varepsilon = 0$.¹⁷⁾ Let us consider a semi-infinite graphene which occupies the region of $y > 0$, and has a zigzag edge at $y = 0$. Assuming that edge sites belong to A sublattice, we adopt the boundary condition of $F_B^\pm(\mathbf{r})|_{y=0} = 0$. The envelope functions for edge states are given as

$$\begin{pmatrix} F_A^\pm(\mathbf{r}) \\ F_B^\pm(\mathbf{r}) \end{pmatrix} = C \begin{pmatrix} e^{\pm ik_x x} e^{-k_x y} \\ 0 \end{pmatrix}, \quad (19)$$

where C is a normalization constant. The absolute value of F_A^\pm in eq. (19) has a maximum value at $y = 0$ and exponentially decays with increasing y . This represents edge states localized along the zz edge. We construct zero-energy wave functions which satisfy the boundary condition of corner edges by using eq. (19).

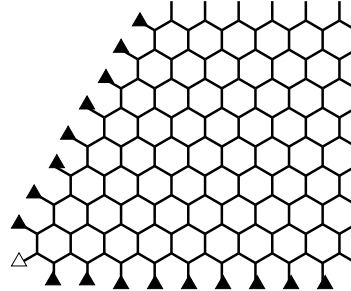


Fig. 11. The boundary condition for the 60° corner edge requires that wave functions vanish at sites marked with a triangle. A site marked with an open triangle belongs to A sublattice, and sites marked with a filled triangle belongs to B sublattice.

(i) 60° corner edge.- We first consider wave functions in the presence of the 60° corner edge as shown in Fig. 11. We attempt to construct wave functions near the K^+ point in terms of two edge localized wave functions. One is the wave function for the 0° zz edge

$$C \begin{pmatrix} e^{-ikx} e^{ik_x(x+iy)} \\ 0 \end{pmatrix}, \quad (20)$$

and the other is the wave function for the 60° zz edge

$$C \begin{pmatrix} e^{-ikx} e^{ik_x(x+iy)e^{i\frac{2}{3}\pi}} \\ 0 \end{pmatrix}, \quad (21)$$

where $K \equiv 4\pi/3a$. Here and hereafter we refer to zz edge intersecting the x axis with angle θ degree as θ° zz edge. We adopt their linear combination

$$\begin{pmatrix} \psi_A(\mathbf{r}) \\ \psi_B(\mathbf{r}) \end{pmatrix} = \begin{pmatrix} e^{-ikx} (C_1 e^{ik_x(x+iy)} + C_2 e^{ik_x(x+iy)e^{i\frac{2}{3}\pi}}) \\ 0 \end{pmatrix} \quad (22)$$

as a trial wave function in the presence of the 60° corner edge. The boundary condition requires that the wave function vanishes at sites marked with triangles in Fig. 11. Because $\psi_B(\mathbf{r}) = 0$, we need to consider only the boundary condition for $\psi_A(\mathbf{r})$. Only the site at the corner with an open triangle belongs to A sublattice. We define this site as the origin of the coordinate. Hence, the boundary condition for $\psi_A(\mathbf{r})$ is simply given by

$$\psi_A(0, 0) = 0, \quad (23)$$

yielding $C_2 = -C_1$. We obtain the wave function in the presence of the 60° corner edge as

$$\begin{pmatrix} \psi_A(\mathbf{r}) \\ \psi_B(\mathbf{r}) \end{pmatrix} = C \begin{pmatrix} e^{-ikx} (e^{ik_x(x+iy)} - e^{ik_x(x+iy)e^{i\frac{2}{3}\pi}}) \\ 0 \end{pmatrix}. \quad (24)$$

This indicates the existence of edge states in the 60° corner edge.¹⁸⁾

(ii) 90° corner edge.- Secondly we consider the 90° corner edge as shown in Fig. 12. In this

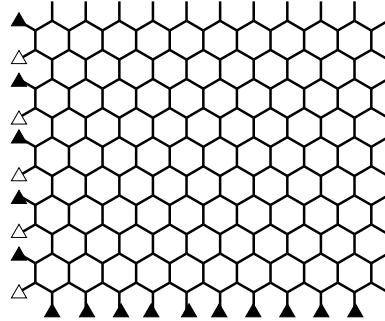


Fig. 12. The boundary condition for 90° corner edge requires that wave functions vanish at sites marked with a triangle. Sites marked with an open triangle belongs to A sublattice, and sites marked with a filled triangle belongs to B sublattice.

case, states near K^+ and K^- points are mixed due to the presence of an ac edge. We construct zero-energy wave functions by using edge localized wave function near the K^+ point,

$$C \begin{pmatrix} e^{-ikx} e^{ik_x(x+iy)} \\ 0 \end{pmatrix}, \quad (25)$$

and that near the K^- point,

$$C \begin{pmatrix} e^{ikx} e^{-ik_x(x-iy)} \\ 0 \end{pmatrix}. \quad (26)$$

We adopt their linear combination

$$\begin{pmatrix} \psi_A(\mathbf{r}) \\ \psi_B(\mathbf{r}) \end{pmatrix} = \begin{pmatrix} C_3 e^{-ikx} e^{ik_x(x+iy)} + C_4 e^{ikx} e^{-ik_x(x-iy)} \\ 0 \end{pmatrix} \quad (27)$$

as a trial wave function. This must vanishes at sites marked with triangles in Fig. 12. Because $\psi_B(\mathbf{r}) = 0$, we need to consider only the boundary condition for $\psi_A(\mathbf{r})$. The sites marked with open triangles belong to A sublattice. We define the site at the corner with an open triangle as the origin. The coordinates of the open triangles are $(x, y) = (0, \sqrt{3}a \times m)$ with $m = 0, 1, 2, \dots$. Hence, the boundary condition for $\psi_A(\mathbf{r})$ reads

$$\psi_A(0, \sqrt{3}a \times m) = 0 \quad (m = 0, 1, 2, \dots). \quad (28)$$

Imposing this condition to ψ_A in eq. (27), we obtain $C_4 = -C_3$. We obtain the wave function for the 90° corner edge as

$$\begin{pmatrix} \psi_A(\mathbf{r}) \\ \psi_B(\mathbf{r}) \end{pmatrix} = C \begin{pmatrix} e^{-ikx} e^{ik_x(x+iy)} - e^{ikx} e^{-ik_x(x-iy)} \\ 0 \end{pmatrix}. \quad (29)$$

This indicates the existence of edge states in the 90° corner edge.

(iii) 150° corner edge.- Thirdly we consider the 150° corner edge as shown in Fig. 13. We obtain zero-energy wave functions using a conformal mapping technique.¹⁹⁾ In terms of the

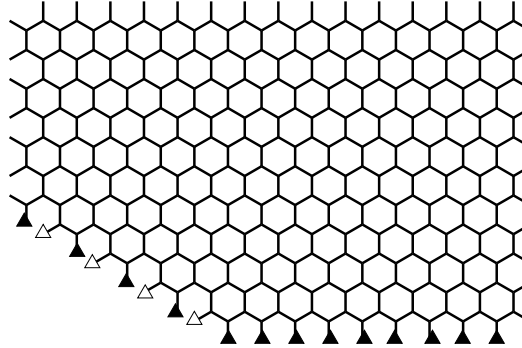


Fig. 13. The boundary condition for the 150° corner edge requires that wave functions vanish at sites marked with a triangle. Sites marked with an open triangle belongs to A sublattice, and sites marked with a filled triangle belongs to B sublattice.

complex variable $z \equiv x + iy$, eq. (19) is rewritten as

$$\begin{pmatrix} F_A^+(z) \\ F_B^+(z) \\ F_A^-(z) \\ F_B^-(z) \end{pmatrix} = \begin{pmatrix} Ce^{ik_x z} \\ 0 \\ C'e^{-ik_x z^*} \\ 0 \end{pmatrix}, \quad (30)$$

where z^* is the complex conjugate of z . Here we introduce the transformation of $w = z^{3/5}$. This transformation maps a 150° corner on z plane to a 90° corner on w plane and vice versa. Thus, the wave function for the 90° corner edge on w plane

$$\begin{pmatrix} \psi_A(w) \\ \psi_B(w) \end{pmatrix} = C \begin{pmatrix} e^{-iKx} e^{ik_x w} - e^{iKx} e^{-ik_x w^*} \\ 0 \end{pmatrix} \quad (31)$$

is mapped to

$$\begin{pmatrix} \psi_A(\mathbf{r}) \\ \psi_B(\mathbf{r}) \end{pmatrix} = C \begin{pmatrix} e^{-iKx} e^{ik_x z^{3/5}} - e^{iKx} e^{-ik_x z^{*3/5}} \\ 0 \end{pmatrix} \quad (32)$$

$$= C \begin{pmatrix} e^{-iKx} e^{ik_x(x+iy)^{3/5}} - e^{iKx} e^{-ik_x(x-iy)^{3/5}} \\ 0 \end{pmatrix} \quad (33)$$

on z plane. The boundary condition requires that the wave function vanishes at sites marked with triangles in Fig. 13. Again, we need to consider only the boundary condition for $\psi_A(\mathbf{r})$. The sites marked with open triangles belong to A sublattice. We define the site at the corner with an open triangle as the origin. The coordinates of the open triangles are $(x, y) = (-\frac{3}{2}a \times m, \frac{\sqrt{3}}{2}a \times m)$ with $m = 0, 1, 2, \dots$. Hence, the boundary condition for $\psi_A(\mathbf{r})$ is given by

$$\psi_A(-\frac{3}{2}a \times m, \frac{\sqrt{3}}{2}a \times m) = 0 \quad (m = 0, 1, 2, \dots). \quad (34)$$

The wave function ψ_A in eq. (33) satisfies this condition. Therefore eq. (33) can be considered

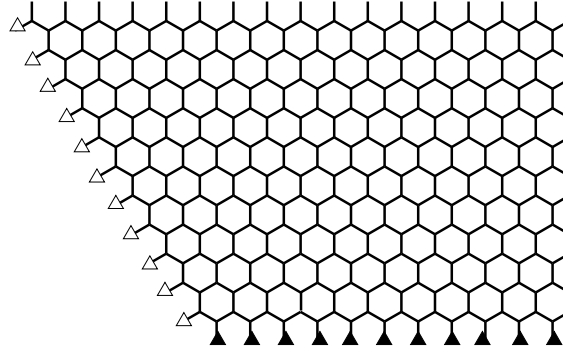


Fig. 14. The boundary condition for the 120° corner edge requires that wave functions vanish at sites marked with a triangle. Sites marked with an open triangle belongs to A sublattice, and sites marked with a filled triangle belongs to B sublattice.

as a wave function in the presence of the 150° corner edge. This indicates the existence of edge states. The envelope functions $e^{ik_x(x+iy)\frac{3}{5}}$ and $e^{-ik_x(x-iy)\frac{3}{5}}$ are different from ordinary envelope functions given in eq. (19), but both satisfy the $\mathbf{k} \cdot \mathbf{p}$ equation given in eq. (18).

(iv) 120° corner edge.- Lastly we consider the 120° corner edge as shown in Fig. 14. The boundary condition requires that $\psi_B(\mathbf{r})$ vanishes at sites marked with a filled triangle and $\psi_A(\mathbf{r})$ vanishes at sites marked with an open triangle. Therefore, both $\psi_A(\mathbf{r})$ and $\psi_B(\mathbf{r})$ are subjected to the boundary condition, in contrast to the 60° case where one component is free from the boundary condition. This crucially affects zero-energy states in the 120° case as we see below. Similar to the treatment for the 60° case, we first adopt a linear combination of the wave function for the 0° zz edge and that for the 120° zz edge as a trial wave function. The wave function for the 0° zz edge near the K^+ point is

$$C \begin{pmatrix} e^{-iKx} e^{ik_x(x+iy)} \\ 0 \end{pmatrix} \quad (35)$$

and the wave function for the 120° zz edge near the K^+ point is

$$C \begin{pmatrix} 0 \\ e^{-iKx} e^{-ik_x(x-iy)} e^{-i\frac{\pi}{3}} \end{pmatrix}. \quad (36)$$

The former has only the A-sublattice component, while the latter has only the B-sublattice component. Obviously, their linear combination does not satisfy the boundary condition for both the A-sublattice and B-sublattice components. We next consider a linear combination of the 0° edge wave functions near the K^+ and K^- points,

$$\begin{pmatrix} \psi_A(\mathbf{r}) \\ \psi_B(\mathbf{r}) \end{pmatrix} = \begin{pmatrix} C_5 e^{-iKx} e^{ik_x(x+iy)} + C_6 e^{iKx} e^{-ik_x(x-iy)} \\ 0 \end{pmatrix}. \quad (37)$$

This is equivalent to eq. (27). Though ψ_B of eq. (37) satisfies the boundary condition, ψ_A cannot satisfy the boundary condition for arbitrary C_5 and C_6 . Finally, we consider a linear

combination of the 0° zz edge wave function and an arbitrary evanescent wave function near the K^\pm point given by

$$C \begin{pmatrix} e^{\mp iKx} e^{\pm ip(x \pm iy)e^{\pm i\theta}} \\ 0 \end{pmatrix}. \quad (38)$$

This wave function, reducing to the 0° zz edge wave function when $\theta \rightarrow 0$, satisfies eq. (18) and is bounded for $0 \leq \theta \leq \frac{\pi}{3}$ in the 120° case. Their linear combination

$$\begin{pmatrix} \psi_A(\mathbf{r}) \\ \psi_B(\mathbf{r}) \end{pmatrix} = \begin{pmatrix} C_7 e^{-iKx} e^{ik_x(x+iy)} + C_8 e^{\mp iKx} e^{\pm ip(x \pm iy)e^{\pm i\theta}} \\ 0 \end{pmatrix}. \quad (39)$$

does not satisfy the A-sublattice boundary condition for arbitrary C_7 , C_8 , p , and θ as long as p is sufficiently small.

We failed to construct zero-energy wave functions in the 120° case in the form of a linear combination of the edge states, in striking contrast to the 60° case. It is considered that this corresponds to the disappearance of the LDOS peak at $\varepsilon = 0$ near the corner observed in the numerical result. We suppose that correct zero-energy states consist of zz edge states and complex scattered waves. We point out that the sublattice configuration of two zz edges plays a crucial role in the qualitative difference between the 60° and 120° cases.

In the remaining of this section we briefly consider the behavior of the LDOS shown in Fig. 8, on the basis of the wave functions obtained above. Figure 8 shows the spatial dependence of the LDOS at $\varepsilon = 0$ in the 60° , 90° and 150° cases. We observe that the LDOS on a zz edge is slightly suppressed in the close vicinity of a corner. This should be distinguished from the strong suppression of the LDOS observed near a 120° corner, and is simply accounted for on the basis of the wave functions for zero-energy edge localized states presented in eqs. (24), (29) and (33). We see that due to destructive interference, the amplitude of these wave functions is suppressed in the close vicinity of a corner located at $(x, y) = (0, 0)$ for a sufficiently small k_x . This accounts for the slight suppression of the LDOS.

5. Summary

We have studied electronic states in semi-infinite graphene with a corner edge, focusing on the stability of edge localized states. The 60° , 90° , 120° and 150° corner edges are examined. The 90° and 150° corner edges consist of one zz edge and one ac edge, while the 60° and 120° corner edges consist of two zz edges. We have numerically obtained the local density of states on the basis of a nearest-neighbor tight-binding model by using Haydock's recursion method. We have shown that edge localized states appear along a zz edge of each corner edge structure except for the 120° case. In the 120° case, we have also shown that edge localized states locally disappear near the corner but emerge with increasing the distance from the corner along each zz edge. To provide insight into these behaviors, we have analyzed electronic states at $\varepsilon = 0$ within the framework of an effective mass equation. Except for the 120° case, we

have succeeded to obtain eigenstates of the effective mass equation by forming a superposition of pair of edge localized wave functions for an infinitely long straight zz edge. This indicates the existence of edge localized states, and is consistent with the behavior of the local density of states. Contrastingly, no eigenstate has been obtained in such a simple form in the 120° case. This suggests a possibility that the local disappearance of edge localized states in the 120° case is beyond the effective mass description. Note that although both the 60° and 120° corner edges consist of two zz edges, zero-energy eigenstates of the effective mass equation are obtained only in the former case. We have pointed out that this reflects the fact that two zz edges belong to a same sublattice in the former case while they belong to different sublattices in the latter case.

Acknowledgment

This work was supported in part by a Grant-in-Aid for Scientific Research (C) (No. 21540389) from the Japan Society for the Promotion of Science, and by a Grant-in-Aid for Specially promoted Research (No. 20001006) from the Ministry of Education, Culture, Sports, Science and Technology.

References

- 1) K. S. Novoselov, A. K. Geim, S. V. Morozov, D. Jiang, Y. Zhang, S. V. Dubons, I. V. Grigoriva, and A. A. Firsov: *Science* **306** (2004) 666.
- 2) K. S. Novoselov, A. K. Geim, S. V. Morozov, D. Jiang, M. I. Katsnelson, I. V. Grigorieva, S. V. Dubonos and A. A. Firsov *Nature* **438**, (2005) 197.
- 3) See, for a review, A. H. Castro Neto, F. Guinea, N. M. R. Peres, K. S. Novoselov, and A. K. Geim: *Rev. Mod. Phys.* **81** (2009) 109.
- 4) J. W. McClure: *Phys. Rev.* **104** (1956) 666.
- 5) P. R. Wallace: *Phys. Rev.* **71** (1947) 622.
- 6) Y. Zhang, Y.-W. Tan, H. L. Stormer, P. Kim: *Nature* **438** (2005) 201.
- 7) T. Ando, T. Nakanishi and R. Saito: *J. Phys. Soc. Jpn.* **67** (1998) 2857.
- 8) M. I. Katsnelson, K. S. Novoselov, A. K. Geim: *Nat. Phys.* **2** (2006) 620.
- 9) M. Fujita, K. Wakabayashi, K. Nakada, and K. Kusakabe: *J. Phys. Soc. Jpn.* **65** (1996) 1920.
- 10) Y. Kobayashi, K. Fukui, T. Enoki, K. Kusakabe, and Y. Kaburagi: *Phys. Rev. B* **71** (2005) 193406.
- 11) Y. Niimi, T. Matsui, H. Kambara, K. Tagami, M. Tsukada, and H. Fukuyama: *Phys. Rev. B* **73** (2006) 085421.
- 12) R. Haydock: in *Solid State Physics*, edited by H. Ehrenreich, F. Seitz and D. Turnbull (Academic, New York, 1980), Vol. 35, p. 216.
- 13) M. J. Kelly: in *Solid State Physics*, edited by H. Ehrenreich, F. Seitz and D. Turnbull (Academic, New York, 1980), Vol. 35, p. 296.
- 14) L. C. Davis: *Phys. Rev. B* **28** (1983) 6961.
- 15) S. Wu, L. Jing, Q. Li, Q. W. Shi, J. Chen, H. Su, X. Wang, and J. Yang: *Phys. Rev. B* **77** (2008) 195411.
- 16) J. C. Slonczewski, P. R. Weiss: *Phys. Rev.* **109** (1957) 272.
- 17) K. Wakabayashi: Ph. D. Thesis, University of Tsukuba (2000).
- 18) M. Ezawa: *Phys. Rev. B* **81** (2010) 201402(R).
- 19) C. Iniotakis, S. Graser, T. Dahm, and N. Schopohl: *Phys. Rev. B* **71** (2005) 214508.